

# Integrated Indium Phosphide Coherent Optical Receivers and Transmitters

Leif A Johansson, Steven Estrella, Jeremy Thomas, Sanjay Kumar, Milan Mashanovitch, and  
Jonathon S Barton  
Freedom Photonics, LLC, Goleta, USA

**Abstract**— Freedom Photonics is developing miniature high-speed optical transmitter and receiver technology for optical communications between airborne, ground and satellite stations. Widely tunable chip-scale compact optical transmitters and receivers have been developed, with very small chip footprint achieved ( $0.5 \times 3.5 \text{ mm}^2$  for transmitter,  $1 \times 2.5 \text{ mm}^2$  for receiver). Both the transmitter and receiver chips are being fabricated on the same wafer using the same fabrication steps, and can be produced as a single, monolithic chip. This technology has been realized in a radiation hard Indium Phosphide photonic integration platform. High level of integration eliminates the need for fiber coupling between different sub-elements (laser; optical amplifier; optical modulator; photodetector) which results in very low optical interconnect losses ( $<0.1 \text{ dB}$ ), and high mechanical robustness. These coherent transmitters and receivers are used to demonstrate generation and demodulation of QPSK optical modulation at clock-rates up to 10 GHz, leading to a total channel data rate of 20 Gbps.

**Index Terms**—Photonic Integrated Circuits; Optical Phase Modulation; Optical Communications.

## I. INTRODUCTION

Optical lasercom systems are anticipated to be at the core of implementation of new inter satellite communications links, due to their high link bandwidths, and utilize very directional beams, leading to high link security. To maximize the benefits of lasercom deployment, it is imperative to maximize the use of photonic integration for system implementation, which will yield the minimum size, weight and power of the whole system. Satellite communications links may have dynamic transmission conditions. This particularly applies to non-stationary satellite links where optical link distances may vary greatly. Link power budgets are generally adapted to providing full connectivity at worst link conditions. An ability to dynamically adapt link bandwidth according to link conditions carries the potential of increasing link throughput under good conditions, or extending the reach of the link by adapting lower bandwidth encoding

Freedom Photonics' miniature high-speed optical transmitter and receiver technology would allow for wide bandwidths, up to 100 Gbps per channel. We have developed widely tunable chip-scale compact optical transmitters and receivers, with very small chip footprint achieved ( $0.5 \times 3.5 \text{ mm}^2$  for transmitter,  $1 \times 2.5 \text{ mm}^2$  for receiver, as seen in Figure 1). This

technology has been realized in a radiation hardened Indium Phosphide photonic integration platform. High level of integration removes the need for fiber coupling between different sub-elements (laser; optical amplifier; optical modulator; photodetector) which eliminates  $\sim 1\text{-}5 \text{ dB}$  loss per fiber coupling and results in very low optical interconnect losses ( $<0.1 \text{ dB}$ ) and high mechanical robustness. These coherent transmitters and receivers are designed to generate and demodulate optical vector modulation such as QPSK modulation. They operate at a clock-rate up to 25 GHz, leading to a total channel data rate of 100 Gbps when polarization multiplexed. The transmitters and receivers are widely-tunable, designed to reach any of 50 wavelength channels within the optical C-band. An array of these devices may reach a total throughput up to 5 Tbps.



Figure 1: Monolithically integrated InP coherent receiver and transmitter photonic IC's.

The advantages of using this type of integrated components for satellite communications links are summarized as:

- *Monolithically integrated receiver (including tunable laser)*: Significant reduction in size, weight and power consumption, increased reliability (single package)
- *Coherent receiver*: Shot noise limited, orders of magnitude better sensitivity than practical direct detection systems
- *Immunity to jamming/interference*: Filtering using the integrated laser-local oscillator; nanosecond wavelength switching possible
- *Spectral efficiency*: Phase modulation schemes are more efficient than amplitude modulation; multilevel modulation capability of the chip improves this further.

- *Adaptive modulation capability:* A single transmitter may be modulated at different clock-rates and with different modulation formats, such as PSK, FSK or PPM type optical modulation, which allows great flexibility to adapt for varying link transmission conditions.
- *Redundancy by design capability:* Easy to add redundant modulators/lasers on the same chip
- *1550nm operation:* Weight reduction due to smaller telescope size

## II. ADAPTIVE OPTICAL MODULATION

Optical link budgets are typically generated to deliver a minimum margin at the worst possible link transmission condition. For free-space optical links this leads to restrictions in available data rates and minimum required power. With adaptive optical modulation, channel throughput may be changed with link conditions. This will allow overall improved throughput or reduced required transmitted power.

There are two options for adaptive modulation: flexible data clock rate and flexible modulation format. Figure 2 illustrates the relation between increased clock rates and increased complexity in modulation formats. One or both approaches can be utilized to respond to changing link transmission conditions. The most straight-forward approach is to adjust the data clock rate while keeping the modulation format fixed. The number of required photons per bit remains the same, so by reducing the clock rate, signal to noise ratio (SNR) improves for a fixed received optical power. The challenge using this approach is to implement a clock rate agnostic modulation format. For example, delayed self-homodyne differential DPSK detection is dependent on a physical delay and add demodulator, where the delay corresponds to a fixed clock rate. In contrast, homodyne coherent detection, the approach Freedom Photonics has taken to PSK modulation formats, relies on interfering the received optical signal with an LO laser, which, in combination with a tunable clock-recovery circuit, result in clock rate agnostic operation.

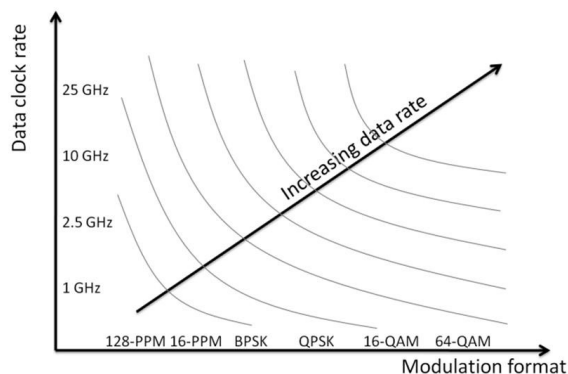


Figure 2: Left: The relation between increased clock-rates and increased complexity in modulation formats. Right: The relation between data throughput and received noise tolerance as the optical modulation format is changed from bandwidth efficient modulation to power efficient modulation, while keeping clock rate constant.

The second alternative is to use adaptive modulation formats. As the received SNR margin increases, one can move to more complex modulation formats with a higher data throughput, such as from BPSK to QPSK to dual polarization QPSK  $\rightarrow$  16-QAM  $\rightarrow$  256-QAM. Conversely, as the SNR is reduced, one utilizes more power-efficient modulation formats including pulse-position modulation (PPM) or multilevel frequency shift keying (M-FSK).

The transmitter and receiver technology Freedom Photonics is developing offers a unique flexibility to pursue different modulation formats. The transmitter contains a full vector modulator, allowing the generation of complex multi-level modulation formats, as well as simple intensity modulation. Likewise, the receiver is a full coherent receiver, allowing detection of the full optical vector information. Furthermore, the transmitter contains a widely tunable sampled-grating laser. This can be tuned to any wavelength within a 40 nm range. More than 100 50GHz-spaced wavelength channels can be reached, allowing encoding in multi-level FSK formats at clock-rates up to 100MHz.

## III. INTEGRATED COHERENT RECEIVER

The monolithically integrated coherent receiver schematic is shown in Figure 3. The chip was realized using photonic integration in indium phosphide (InP). At the center of the chip is a widely tunable sampled grating distributed Bragg reflector (SGDBR) laser, used as the receiver LO, providing 40nm tunability and bandwidth coverage [1]. The signal from the LO is split into two identical paths. In each of the two paths, the LO power is amplified with a semiconductor optical amplifier (SOA), before the signal is routed using 2 total internal reflection (TIR) mirrors with a perpendicular waveguide connecting them. The signal from the second TIR mirror is then guided into a 2x4 multimode interference (MMI) hybrid. The receiver chip has two signal input waveguides, which are used to independently couple each of the two demultiplexed polarization data streams from a polarization multiplexed network data stream. The four outputs of each of the hybrids are separated using S-bend waveguides, which terminate in 4 photodiodes. Thus, the chip is capable of simultaneously detecting two independent data streams from a polarization multiplexed QPSK data stream – however, polarization demultiplexing and rotation of the transverse-magnetic (TM) polarization into transverse-electric (TE) has to be performed external to the chip.

### A. 2x4 MMI Based 90° Optical Hybrid

For our receiver implementation, we utilize 2x4 general interference based MMI 90° hybrids, essential for coherent demodulation [2]. In the general case of an N x N MMI coupler, the modal field distribution at

the input is reproduced in  $N$  self-images at the output, for particular coupler distances. The phase relationship  $\phi_{n,m}$  between an input  $n$  to the output  $m$  are given in [2].

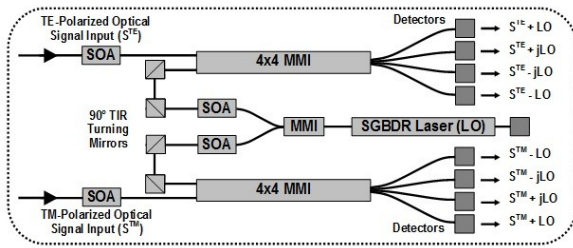


Figure 3: Schematic of our monolithically integrated dual-polarization photonic integrated coherent receiver, including SOAs, MMIs and TIRs.

Since the detectors are unbalanced, the phase relationship from each output detector must be taken into account in order to successfully demodulate using either a digital signal processing (DSP) algorithm or integrated circuits.

### B. Total Internal Reflection Mirrors

One unique feature of this coherent tunable receiver design is the total internal reflection mirrors used to achieve the highly compact device. Compared to some previously reported integrated designs [3,4] which used 2x2 MMI couplers and arrayed waveguide gratings (AWGs), our TIR mirror based integrated device occupies only a 4 mm<sup>2</sup> chip area, even though it includes a single fully tunable local oscillator. A scanning electron micrograph (SEM) picture of a TIR mirror in the integrated coherent receiver is shown in Figure 4. An inductively coupled plasma reactive ion etching (ICP RIE) process is used to fabricate the TIR mirrors. A deep etch forms the vertical facet necessary to achieve total internal reflection at the semiconductor/air interface. The mirror is oversized laterally to reflect the propagating weakly confined optical mode profile [5]. Mirror loss has been measured at 0.4dB/mirror $\pm$ .07dB from an on-wafer test structure.

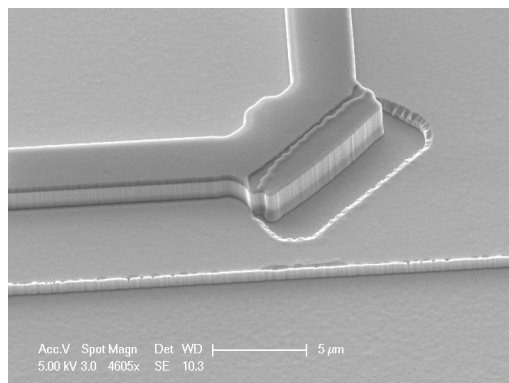


Figure 4: SEM of TIR mirror used in coherent receiver.

### C. Device Fabrication

An impurity-free vacancy-enhanced quantum-well intermix (QWI) process is used to create the active and passive bandgap regions on the chip. The material is selectively ion-implanted with phosphorus ions, and due to the lattice damage caused by the implant, vacancies are created in the material. The vacancies are then diffused through the quantum wells by rapid thermal annealing of the sample. The vacancy diffusion then causes the quantum well and barrier materials to intermix, resulting in an increase in the bandgap. The implanted buffer layer material is then etched away to leave the sample defect free. This process is described in greater detail in [6]. The intermixing process leads to a passive waveguide loss that is low for InP, around 1.5 dB/mm. The bandgap of the non-intermixed region remains stable to provide gain for the laser and the SOAs, or when reverse biased, to provide absorption in the detector regions.

### D. Device Demonstration

Figure 5 shows a photograph of the device mounted on a ceramic carrier containing DC leads, termination resistors for the modulator, capacitors for DC blocking or decoupling, and radio-frequency (RF) coplanar transmission waveguide (CPW) lines. Figure 6 shows overlapped spectra over the full tuning range of the integrated LO laser. The tuning range exceeds 40 nm with an LO output power higher than 20mW over its tuning range. The LO exhibits a linewidth ranging from 15-21MHz, which has been shown to be primarily attributed to high-frequency white noise [7]. In Figure 7, the frequency response of the detectors has been characterized. The 3-dB bandwidth is measured to be 5GHz at -4V detector bias, for a 50  $\mu$ m long waveguide detector, which is sufficient for 10Gbps operation. The inset eye diagram is taken using a 10Gbps non-return-to-zero (NRZ) on-off keyed (OOK) modulated input signal with the LO laser off.

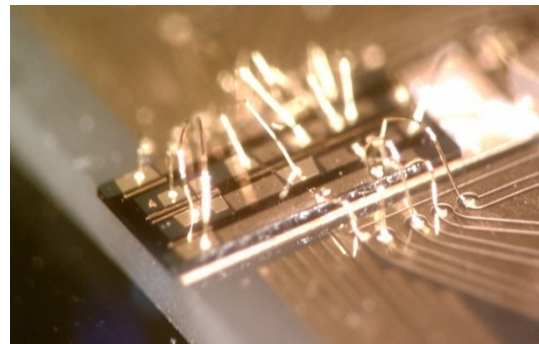


Figure 5: Photograph of the widely tunable optical receiver integrated circuit mounted on an Aluminum-Nitride ceramic carrier.

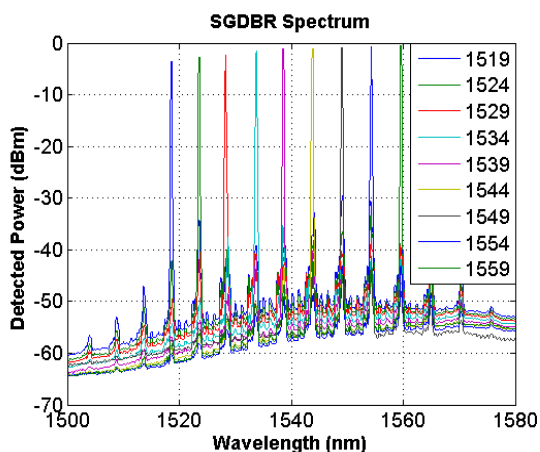


Figure 6: Typical output wavelength spectra over the tuning range of the widely tunable laser obtained from test device.

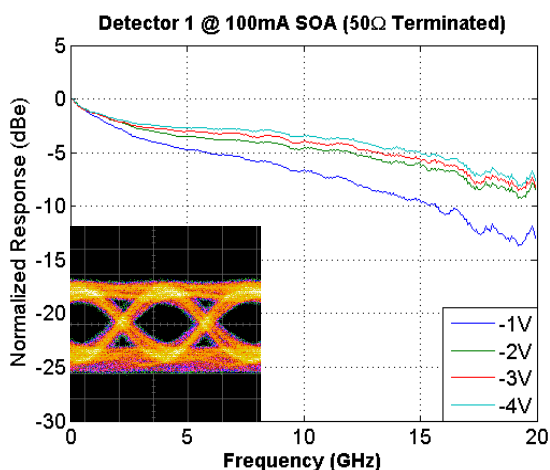


Figure 7: Measured frequency response of a single 50  $\mu\text{m}$  long detector, terminated into 50 $\Omega$ . A detected eye diagram at 10Gbps NRZ is inset.

To demonstrate the performance of the integrated coherent receiver, an optical QPSK link was constructed. Using our tunable coherent receiver chip to detect the optical phase modulation, the detected signal consists of the rapidly varying signal phase added to the more slowly varying random phase difference between signal and LO laser. In this demonstration, demodulation was implemented through QPSK demodulation using a DSP algorithm.



Figure 8: Schematic of proof-of-concept coherent link demonstration, using a 20Gbps QPSK encoded optical signal.

Figure 8 outlines the experimental setup used to measure and quantify the coherent receiver performance. A 10 Gbaud QPSK signal was generated using a 100kHz linewidth external continuous wave (CW) tunable laser source and a lithium niobate

(LiNbO<sub>3</sub>) dual Mach-Zehnder modulator (DMZM). The data for the modulation of both the I and the Q branches originated from the same 10Gbps  $2^{31}-1$  pseudo-random binary sequence (PRBS), with a differential delay between I and Q PRBS signals. This produced an optical data stream with a total bit rate of 20Gbps (10Gbaud). The signal was then coupled into a single arm of our integrated coherent receiver using a polarization rotator and lensed fiber. For the first experiment, the external laser was tuned to the untuned frequency of the integrated SGDBR LO, determined by zero bias applied to front and back mirrors and phase section. A DC bias of -3V was applied to each detector, and the measured RF photocurrent of each differential I and Q component was captured by a high-bandwidth optical modulation analyzer. Subsequent measurements were made at different wavelengths, by tuning both LO and external laser, and captured using a real-time oscilloscope.

The sampled waveforms from the coherent receiver were then passed through a DSP algorithm, which adjusts each IQ component through amplitude equalization, bit retiming, and carrier phase tracking. The resulting constellation diagrams at 10 Gbaud, for three different input wavelengths, are shown in Figure 9.

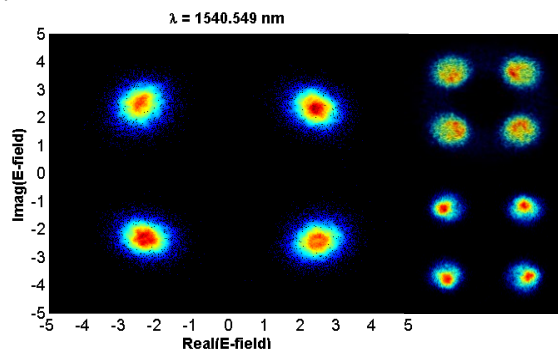


Figure 9: Constellation diagrams obtained at 1540 nm (left), 1530 nm (upper right), and 1550 nm (lower right) from coherent link demonstration using a 20 Gbps QPSK encoded optical signal using  $2^{31}-1$  PRBS, after DSP post processing. Linear color coding corresponds to symbol density.

#### IV. INTEGRATED OPTICAL TRANSMITTER

The monolithically integrated coherent transmitter schematic is shown in Figure 10. The chip was realized using photonic integration in indium phosphide (InP). At the beginning of the chip is a widely tunable sampled grating distributed Bragg reflector (SGDBR) laser, used as the LO, providing 40nm tunability and bandwidth coverage [1]. The signal from the LO is amplified with a semiconductor optical amplifier (SOA), before the signal is split into 4 paths, using a 1x4 multimode interference (MMI) splitter. The light in each path is sent through a static phase adjustment electrode embedded in the S-bent waveguides, which is essential for setting the MZMs in the quadrature state. The high-speed MZMs are

formed using 400 $\mu\text{m}$  long quantum-well intermixed (QWI) regions, with a photoluminescence (PL) peak at 1.5 $\mu\text{m}$ , utilizing the quantum-confined Stark effect (QCSE) for light absorption. After the light in each of the four arms is modulated, it is recombined in a 4x3MMI, which allows for the monitoring the MZM in the OFF state. Thus, the chip is capable of transmitting a single transverse-electric (TE) polarization QPSK data stream in a compact footprint.

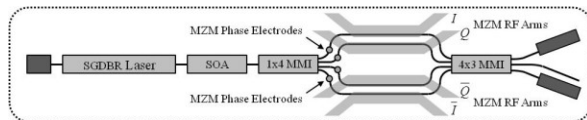


Figure 10: Schematic of our monolithically photonic integrated coherent transmitter, including SOAs, nested MZMs, and absorbers.

### A. 1x4 & 4x3 MMI Based Nested Mach-Zehnder Modulator

For our compact transmitter implementation, we utilize 1x4 and 4x3 general interference based MMIs, critical to forming a small footprint nested MZM modulator. The 2 MZMs in parallel rely on static phase electrodes to adjust the optical phase to the optimal operation point for QPSK encoding. Since the 1x4 MMI is a balanced power splitter, the applied current for each phase electrode induces additional loss, which appears as a slight quadrature imbalance. This imbalance from the phase electrodes can be compensated for by altering the reverse bias applied to the QWI modulator sections.

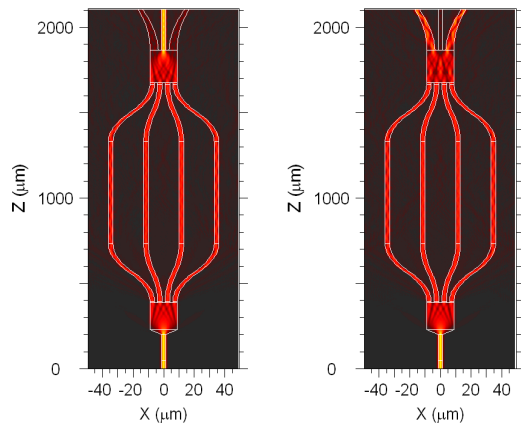


Figure 11: (left) Modulator in the ON state, with relative phase in the four waveguides of 0, +90, +90, 0 degrees in the respective branches (right) Modulator in the OFF state.

In the OFF state of the nested MZM, light is equally split between the outside waveguides, providing phase feedback of the modulator. In Figure 11, beam propagation simulations of the structure are shown, with optimal phase configurations in the respective branches to achieve the ON state and OFF state, with >25dB theoretical extinction.

### B. Device Demonstration

Figure 12 shows a photograph of the device mounted on a ceramic carrier containing DC leads,

termination resistors for the modulator, capacitors for DC blocking, and radio-frequency (RF) coplanar transmission waveguide (CPW) lines. The tuning range of the integrated laser exceeds 40 nm with an output power higher than 20mW over its tuning range. In Figure 13, the frequency response of the modulators (including carrier) has been characterized. The average 3-dB bandwidth is measured to be 8GHz at -3V bias, for a 400 $\mu\text{m}$  long waveguide modulator, which is sufficient for 10Gbps operation. The inset eye diagram is taken using a 20Gbps non-return-to-zero (NRZ) QPSK modulated output signal.

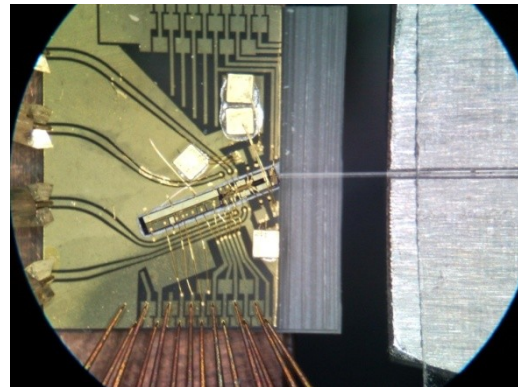


Figure 12: Photograph of the widely tunable optical transmitter integrated circuit mounted on an Aluminum-Nitride ceramic carrier.

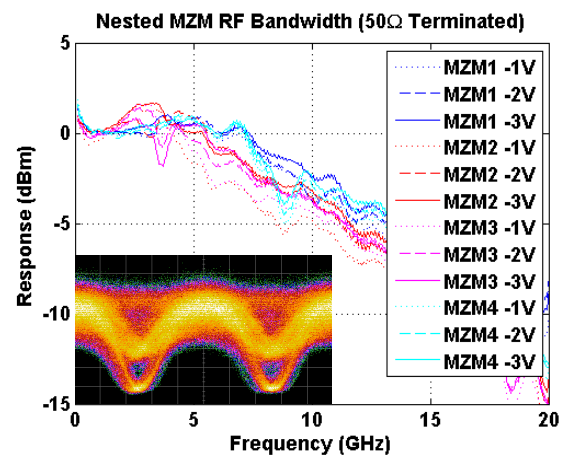


Figure 13: Measured frequency response of a single 400 $\mu\text{m}$  long modulator, terminated into 50 $\Omega$ . A detected eye diagram for 20Gbps NRZ QPSK is inset.

To demonstrate the performance of the integrated transmitter, an optical QPSK link was constructed. Figure 14 outlines the experimental setup used to measure and quantify the coherent transmitter performance. The data for the modulation of both the I and the Q branches originated from the same 10Gbps  $2^{31}-1$  pseudo-random binary sequence (PRBS), with a differential delay between I and Q PRBS signals to generate a pseudo-random quaternary sequence (PRQS). Bit alignment was controlled by line extenders to ensure proper phase delay through all coaxial cables, connectors, amplifiers, and bias-

tees, producing an optical data stream with a total bit rate of 20Gbps (10Gbaud). The differential I and Q signals were then coupled into each arm of the nested MZMs on our integrated coherent transmitter using a 4 ground-signal-ground (GSG) style RF probe. With the MZMs operating in the quadrature state by adjusting all phase electrodes, a  $5V_{p-p}$  AC signal with a DC bias of  $-3V$  was applied to each modulator. The output optical waveform was captured by a high-bandwidth optical modulation analyzer (OMA), and demodulated into a single-ended I and Q voltage waveform. Measurements were captured at different wavelengths, requiring the tuning of both the integrated SGDBR laser and the LO laser within the OMA. Proper frequency tuning was ensured by measuring the RF beat spectrum on a high-bandwidth electrical spectrum analyzer (ESA), not shown in the experiment schematic.

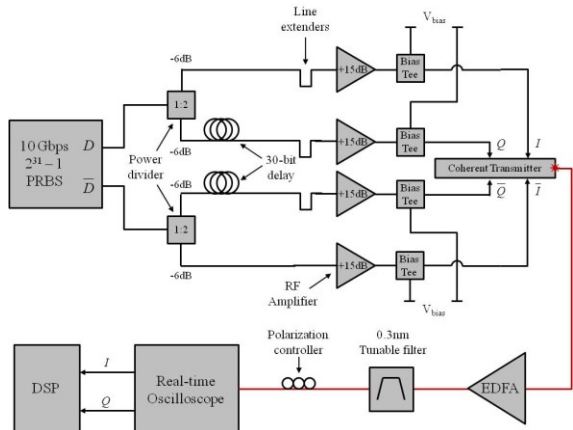


Figure 14: Schematic of proof-of-concept coherent link demonstration, using a 20Gbps QPSK encoded optical signal.

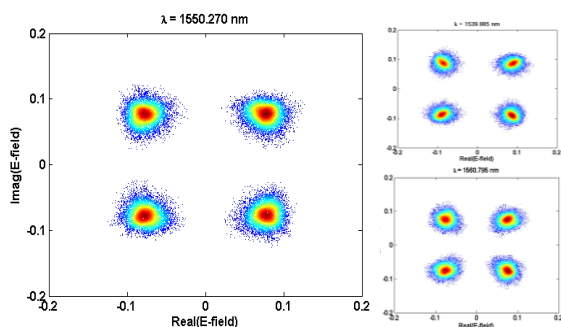


Figure 15: Constellation diagrams obtained at 1540 nm (top), 1550 nm (left), and 1560 nm (bottom) from coherent link demonstration using a 20 Gbps QPSK encoded optical signal using  $2^{31}-1$  PRBS, after DSP post processing. Linear color coding corresponds to symbol density.

The sampled waveforms from the coherent transmitter were then passed through a DSP algorithm, which adjusts the IQ component through amplitude equalization, bit retiming, and carrier phase tracking. The resulting constellation diagrams at 10Gbaud (20Gbps), for three different output wavelengths, are shown in Figure 15.

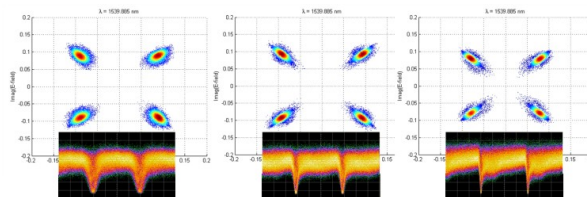


Figure 16: QPSK constellation density plots at 1540nm for (left) 5GHz, (center) 2.5GHz, and (right) 1.25GHz.

A second experiment was conducted in which the clock-rate was adjusted down to 5, 2.5, and 1.25GHz. The purpose in the experiment is to demonstrate the adaptive clock-rate behavior of the PIC, decreasing the clock frequency when the SNR has decreased. Eye diagrams for QPSK modulation at 5, 2.5, and 1.25GHz are shown in Figure 16 together with resultant QPSK constellation density plots, indicating the ability to dynamically change the clock-rate.

### C. Pulse-Position Modulation Demonstration

Pulse-position modulation (PPM) provides improved sensitivity in terms of photons/bit compared to standard binary modulation formats. This leads to higher throughput under difficult transmission conditions, where received power is limited. PPM was implemented by connecting the electrical output from a Xilinx ML605 evaluation board, with an onboard Virtex-6 FPGA, to the SOA following the laser, instead of a modulator. This allows more efficient generation of optical power, as an optical modulator would be biased for extinction for the majority of time, therefore wasting most of the output from the SOA.

The FPGA board was programmed to generate a specific repeating pattern (frame) of pulses, with each pulse 0.8ns wide. The pattern was hard-coded in the RAM of the Virtex-6 FPGA and chosen such that the resulting pulses were of PPM format.

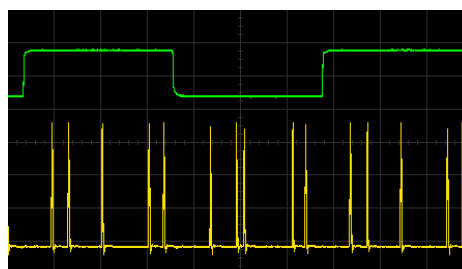


Figure 17: (Bottom) Repeating bit frame consisting of 10 16-PPM symbols (top) trigger signal that goes high at the start of each pattern.

The FPGA board has two pairs of differential SMA output ports, one of which is designed to support high-speed data rates. The high speed pair of ports is used to transmit the PPM data to the SOA of the laser, while the other pair is used to generate a trigger signal used to capture the resulting optical data on the oscilloscope. A screenshot of the captured electrical bit pattern, along with the trigger signal, are shown in Figure 17. The 16-PPM electrical sequence was

generated with only 10 symbols per frame, with 1.5 frames displayed in the screenshot.

16-PPM is achieved by modulating a semiconductor optical amplifier (SOA) to generate high peak-power pulses. The PPM symbols are distinguished by the relative difference in time between successive received pulses. A schematic of the PPM link is shown in Figure 18, including the FPGA to generate the electrical pulses, and an RF amplifier to increase the pulse amplitude before going into the SOA. The oscilloscope used to capture the optical pulses is not shown in the schematic.

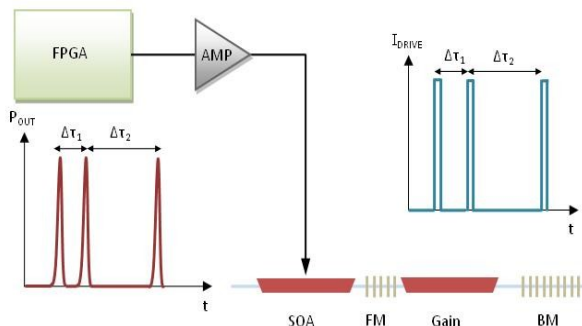


Figure 18: PPM demonstration link schematic

The 0.8ns wide PPM electrical waveforms were generated from an FPGA board, and amplified with a limiting RF amplifier. Optical PPM waveforms from the fiber-coupled output of the transmitter were captured by an oscilloscope and are shown in Figure 19. The 0.8ns optical pulses correspond to a frequency of 1.25GHz, which is a frame frequency of 78.125MHz, or a 312.5Mbps data rate. A continuous-wave (CW) fiber-coupled output of 1.2mW was measured, corresponding to a peak power around 19.2mW.

In addition to demonstrating PPM modulation at a single wavelength, we have also demonstrated the ability to widely tune the optical output across the C-band. The laser can be tuned approximately 40nm through the C-band, with optical PPM waveforms captured at 1532nm, 1545nm, 1551nm, 1558nm, 1564nm, and 1570nm demonstrated.

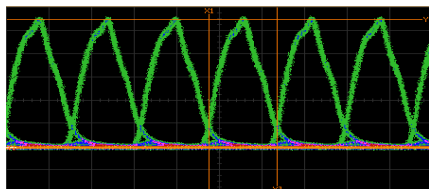


Figure 19: PPM optical waveforms at 6 different wavelengths, covering 40nm in the C-band

#### D. Optical Frequency Shift Keying

Frequency Shift Keying (FSK) is generated by encoding data by switching the carrier center frequency. In the optical domain, this may be achieved using a tunable laser source. Several methods for demodulation may be applied. One design would involve an optical wavelength

demultiplexer and a receiver array, each which would receive a signal similar to a single-channel PPM modulated signal. For this initial demonstration, simple binary FSK was demonstrated. However, for ~50nm wavelength range, 64-FSK would be available using a standard 100 GHz wavelength spacing.

A schematic of the 2-FSK experiment is shown in Figure 20, including the Spartan FPGA and interface board. With the output current to the front mirror changing between two levels, it is expected that two lasing modes will be produced over time, switching from one to the other at the clock rate. An optical tunable filter was then used to select the appropriate wavelength of interest, which would be replaced by an AWG once the appropriate injected current levels are selected to produce an optical output within the specified pass-band.

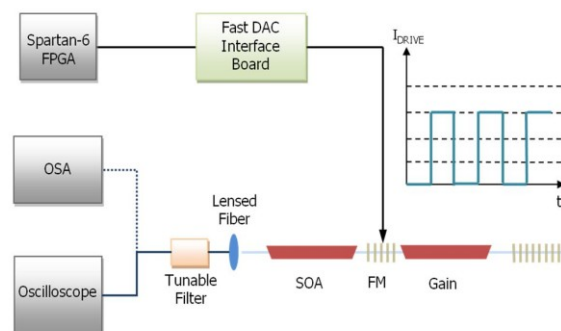


Figure 20: Schematic of experimental demonstration for 2-FSK modulation

The experimental FSK controller platform consists of a Xilinx Spartan-6 FPGA and three fast-switching digital-to-analog converter (DAC) current sources that are mounted on a custom board. For this demonstration a single fast DAC channel was used to supply current to the front mirror of the tunable transmitter. A clock rate of 5.86MHz is used to demonstrate 2-FSK, resulting in a data rate of 5.86Mbps.

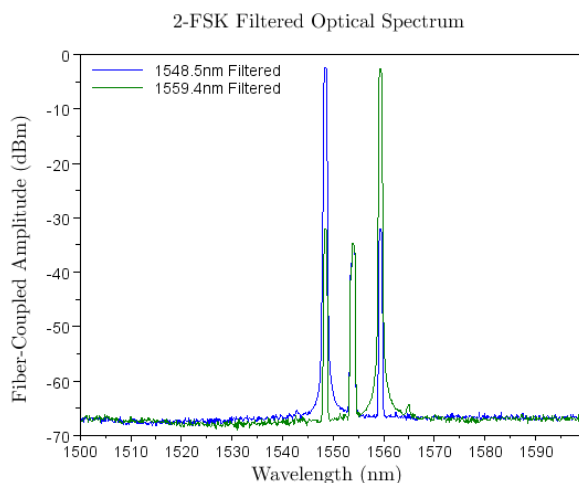


Figure 21: 2-FSK filtered modulation by overlaid optical spectrum

With the output of the DAC directly connected to the front mirror of the EML, the overlaid output

spectra captured by the OSA is shown in Figure 21. From the filtered optical spectra, the intermediate mode in between the two switching modes is apparent, formed by the slow rise/fall time of the DAC output. An output spectrum through a tunable filter was taken for each of the desired wavelength channels in the 5.86MHz 2-FSK modulation experiment, and is shown in Figure 21. From the spectra, the side-mode suppression ratio (SMSR) of the adjacent “intermediate mode” to the desired operating wavelength channel is approximately 32dB, slightly higher than the SMSR to the second wavelength channel at approximately 30dB.

The resulting filtered optical waveforms for the 2-FSK modulation experiment are shown in Figure 22. In the time domain, it is possible to see the wavelength distribution per digital bit. At the zero current level (untuned), the resulting waveform exhibits a 50% duty cycle as expected, however it is on the transitions to the desired tuned wavelengths that lasing mode hops occur.

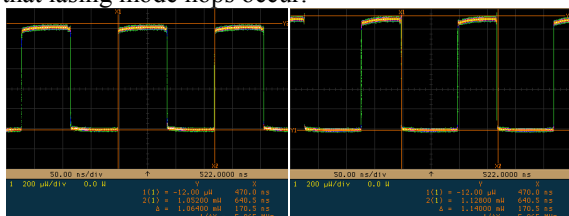


Figure 22: Filtered Optical time-domain waveforms of 5.86MHz 2-FSK modulation captured at (top) 1548.5nm (center) 1554.1nm and (bottom) 1559.4nm

## V. CONCLUSION

In the preceding, results for miniature high-speed optical transmitter and receiver technology for optical communications between airborne, ground and satellite stations have been shown. Widely tunable chip-scale compact optical transmitters and receivers have been developed, with very small chip footprint achieved (0.5x3.5mm<sup>2</sup> for transmitter, 1x2.5mm<sup>2</sup> for receiver). Both the transmitter and receiver chips are being fabricated on the same wafer using the same fabrication steps, and can be produced as a single, monolithic Indium Phosphide chip. These coherent transmitters and receivers have been demonstrated to generate and demodulate QPSK optical modulation at clock-rates up to 10 GHz, leading to a total channel data rate of 20 Gbps. The transmitters and receivers are widely-tunable, designed to reach any of 50 wavelength channels within the optical C-band.

Further, pulse-position modulation and optical frequency shift keying have been demonstrated for power constrained optical links. It is envisioned that adaptive optical modulation could be achieved, using a single transmitter to transmit a range of optical modulation formats at different bit rates, each optimized for varying link transmission conditions.

## VI. REFERENCES

- [1] V. Jayaraman, Z. Chuang, and L. Coldren, “Theory, Design, and Performance of Extended Tuning Range Semiconductor Lasers with Sampled Gratings,” *IEEE J. Quantum Electron.*, vol. 29, pp. 1824-1834, June 1993.
- [2] M. Seimetz and C.-M. Weinert, “Options, Feasibility, and Availability of 2x4 90° Hybrids for Coherent Optical Systems,” *J. Lightwave Technol.* 24(3), 1317-1322 (2006).
- [3] V. E. Houtsma, N. Weimann, T. Hu, R. Kopf, A. Tate, J. Frackoviak, R. Reyes, Y. Chen, C. R. Doerr, L. Zhang, and D. Neilson, “Manufacturable Monolithically Integrated InP Dual-Port Coherent Receiver for 100G PDM-QPSK Applications,” in *Optical Fiber Communication Conference, OSA Technical Digest (CD)* (Optical Society of America, 2011), paper OML2.
- [4] R. Nagarajan, D. Lambert, M. Kato, V. Lal, G. Goldfarb, J. Rahn, M. Kuntz, J. Pleumeekers, A. Dentai, H. Tsai, R. Malendevich, M. Missey, K. Wu, H. Sun, J. McNicol, J. Tang, J. Zhang, T. Butrie, A. Nilsson, M. Reffle, F. Kish, and D. Welch, “10 Channel, 100Gbit/s per Channel, Dual Polarization, Coherent QPSK, Monolithic InP Receiver Photonic Integrated Circuit,” in *Optical Fiber Communication Conference, OSA Technical Digest (CD)* (Optical Society of America, 2011), paper OML7.
- [5] D. G. Kim, C. Ozturk, J. H. Shin, J. C. Yi, and N. Dagli, “Self-aligned total internal reflection mirrors with very low loss,” in *Optical Amplifiers and Their Applications/Integrated Photonics Research, Technical Digest (CD)* (Optical Society of America, 2004), paper IThG5.
- [6] E. J. Skogen, J. S. Barton, S. P. Denbaars, and L. A. Coldren, “A quantum-well-intermixing process for wavelength-agile photonic integrated circuits,” *IEEE J. Sel. Topics Quantum Electron* 8(4), 863–869 (2002).
- [7] S. Nakagawa, G. A. Fish, A. Dahl, P. C. Koh, C. Schow, M. Mack, L. Wang, and R. Yu, “Phase Noise of Widely-Tunable SG-DBR Laser,” in *Optical Fiber Communication Conference, Technical Digest* (Optical Society of America, 2003), paper ThF2.